

NJC

Accepted Manuscript



This is an *Accepted Manuscript*, which has been through the Royal Society of Chemistry peer review process and has been accepted for publication.

Accepted Manuscripts are published online shortly after acceptance, before technical editing, formatting and proof reading. Using this free service, authors can make their results available to the community, in citable form, before we publish the edited article. We will replace this *Accepted Manuscript* with the edited and formatted *Advance Article* as soon as it is available.

You can find more information about *Accepted Manuscripts* in the [Information for Authors](#).

Please note that technical editing may introduce minor changes to the text and/or graphics, which may alter content. The journal's standard [Terms & Conditions](#) and the [Ethical guidelines](#) still apply. In no event shall the Royal Society of Chemistry be held responsible for any errors or omissions in this *Accepted Manuscript* or any consequences arising from the use of any information it contains.

Interaction of Nd(III) and Cm(III) with borate in dilute to concentrated alkaline NaCl, MgCl₂ and CaCl₂ solutions: solubility and TRLFS studies

Katja Hinz^{1*}, Marcus Altmaier¹, Xavier Gaona¹, Thomas Rabung¹, Dieter Schild¹, Michael Richmann², Donald Reed², Evgeny Alekseev³, Horst Geckeis¹

¹Institute for Nuclear Waste Disposal, Karlsruhe Institute of Technology, P.O. Box 3640, 76021 Karlsruhe, Germany

²Los Alamos National Laboratory, Repository Science and Operations, Carlsbad, NM 88220, USA

³Institute of Energy and Climate Research (IEK-6), Forschungszentrum Jülich, 52428 Jülich, Germany

Abstract

The interaction of lanthanides and trivalent actinides with borate in dilute to concentrated alkaline NaCl, MgCl₂ and CaCl₂ solutions was investigated at $22 \pm 2^\circ\text{C}$ by a comprehensive series of solubility experiments with Nd(OH)₃(am), and complemented with Cm(III)-TRLFS studies (TRLFS: time resolved laser fluorescence spectroscopy) under analogous pH and ionic strength conditions. Although there was clear evidence of borate complexation in the pH range of 8.5 to 10, overall no significant increase in Nd(III) solubility occurred in any of the investigated salt systems in the presence of $[\text{B}]_{\text{tot}} \leq 0.4 \text{ M}$, compared with analogous borate-free solutions. On the contrary, a significant decrease in Nd(III) concentration was observed at $\text{pH}_c \leq 9$ in NaCl and MgCl₂ systems with $[\text{B}]_{\text{tot}} \geq 0.16 \text{ M}$ (diluted salt systems) or $[\text{B}]_{\text{tot}} \geq 0.04 \text{ M}$ (concentrated salt systems). This observation, together with a clear change in the slope of the solubility curve and the further confirmation by XPS analyses, indicates the transformation of Nd(OH)₃(am) into a so far unknown Nd(III)-borate solid phase with significantly lower solubility. Similar Nd(III) concentrations in the aqueous phase are obtained in undersaturation solubility experiments conducted with a synthesized crystalline phase Nd[B₉O₁₃(OH)₄](cr). TRLFS confirmed the formation of aqueous Cm(III)-borate complexes in dilute to concentrated NaCl and MgCl₂ systems at $\text{pH}_c = 8$ and $[\text{B}]_{\text{tot}} \geq 0.04 \text{ M}$. Two different Cm(III)-borate species are proposed based on the peak shift of the spectra, although the resulting fluorescence emission bands do not allow the definition of an unequivocal chemical model for this system. TRLFS also shows that no Cm(III)-borate complexes form under hyperalkaline conditions ($\text{pH}_c = 12$), due to the stronger competition

* Corresponding author e-mail: katja.hinz@kit.edu, marcus.altmaier@kit.edu

posed by hydrolysis and the predominance of weakly coordinating $B(OH)_4^-$ in the aqueous phase. These results show the impact of An(III)–borate interactions on An(III) speciation and highlight the hitherto unknown role of borate in the immobilization of trivalent actinides under repository-relevant conditions due to the formation of borate-bearing solid phases with significantly lower solubility than the corresponding hydroxides.

Keywords: neodymium; curium; borate; solubility; TRLFS; solid phase transformation

1. Introduction

The prediction of the long term safety of a repository for nuclear waste disposal needs detailed understanding of the chemistry and migration behavior of actinides. Waste disposal facilities in deep underground geological repositories excavated in rock-salt formations are currently operative (i.e. Waste Isolation Pilot Plant (WIPP), New Mexico, USA) or under consideration¹. Although exceptionally dry conditions are expected in rock-salt formations, concentrated NaCl and MgCl₂ brines may occur in the unlikely event of water intrusion into the repository. Corrosion of cementitious waste forms in MgCl₂ brines can further lead to CaCl₂-dominated solutions with $\text{pH}_c \leq 12$ ². Strongly reducing conditions are expected in deep underground repositories due to the anoxic corrosion of the iron and steel used as canister or construction material, leading to the removal of oxygen, formation of dissolved Fe²⁺ and Fe(II) minerals, and the generation of H₂. Under these conditions, trivalent +III and tetravalent +IV oxidation states will dominate the aqueous chemistry of actinides. Boron can be present in repositories for radioactive waste disposal as a component in the emplaced waste inventory. In repositories in rock-salt formations, boron can further be a component of the intruding brine solutions. Very large borax (Na₂B₄O₅·8H₂O) deposits have been reported at the Salado rock-salt formation where the WIPP is located, which lead to relatively high boron concentrations (up to 0.045 M)³.

Although the aqueous chemistry of An(III) and An(IV) under repository-relevant conditions is mostly dominated by hydrolysis reactions, the role of other inorganic and organic ligands in complexing (and thus potentially mobilizing) actinides needs to be assessed properly. In contrast to carbonate, phosphate or sulphate, little attention has been dedicated so far to the possible complexation of borate species with actinides^{3, 4}. The lack of experimental studies assessing An–borate complexation is well-reflected in the publications of the OECD Nuclear Energy Agency thermodynamic database project (NEA–TDB), where no aqueous borate species or solid compounds are selected for any of the actinides evaluated (U, Np, Pu, Am, Th)^{5, 6}. Borkowski and co-workers assessed the effect of borate on Nd(III) solubility in dilute to concentrated NaCl solutions at $\text{pH}_c = 8.6$ and $0 \leq [\text{B}]_{\text{tot}} \leq 0.16 \text{ M}$ ³. The authors observed a slight increase in Nd concentration (in the range of $5.0 \cdot 10^{-8} \text{ M} - 2.5 \cdot 10^{-7} \text{ M}$) as a function of $[\text{B}]_{\text{tot}}$, ionic strength and pH which was related to the formation of a NdHB₄O₇²⁺-complex. Borkowski and co-workers derived chemical and thermodynamic models assuming a boron speciation dominated by the species HB₄O₇⁻ under the particular conditions of their

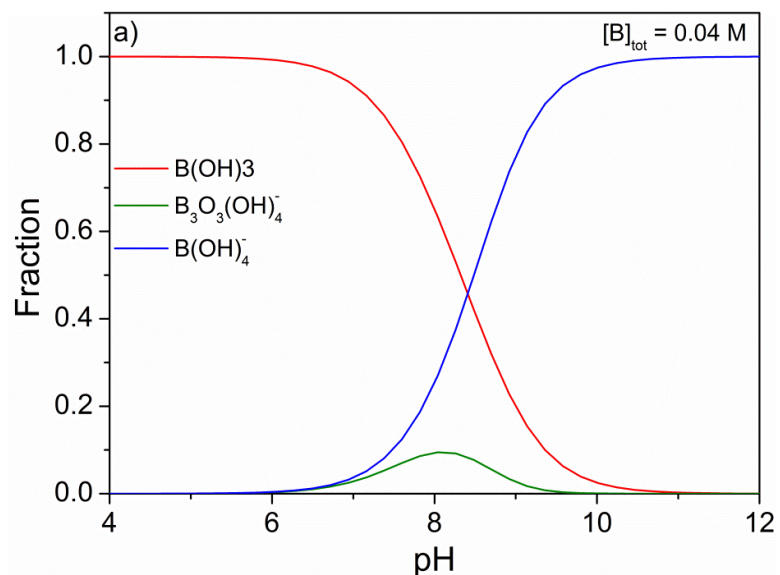
experiments. Recently, Schott et al. investigated the interaction of Eu(III) with borate in aqueous solution⁷. TRLFS experiments confirmed a weak Eu(III)–borate complexation at pH < 6. At pH ~6 and in the presence of high boron concentrations ($0.3 \text{ M} \leq [\text{B}]_{\text{tot}} \leq 0.7 \text{ M}$), the authors observed the formation of a Eu(III)–borate solid phase. The solid was characterized by XRD, IR and solid-state TRLFS, although these techniques provided inconclusive information on the stoichiometry of the newly formed compound. Kienzler et al. performed leaching experiments with simulated borosilicate glass doped with U(IV), U(VI), Pu(IV), Am(III), Np(IV) and Np(V) in concentrated NaCl solutions. Experiments were performed within $7.5 \leq \text{pH}_c \leq 8.5$ at $T = 110^\circ\text{C}$ and 190°C ⁸. The authors observed no enhanced release of radionuclides in spite of the high borate concentration in solution ($\sim 10^{-2} \text{ mol}\cdot\text{kg}^{-1}$). Chernorukov, Nipruk and co-workers⁹⁻¹⁹ conducted a very comprehensive series of thermochemical and solubility experiments with $\text{M}^{\text{I,II}}\text{-U(VI)-B}$ solid phases, with $\text{M}^{\text{I}} = \text{Li, Na, K, Rb, Cs}$ and $\text{M}^{\text{II}} = \text{Mg, Ca, Sr, Ba, Mn, Co, Ni, Zn}$. The uranoborates were prepared by a combination of hydrothermal and ion-exchange approaches. The authors reported both $\log K_s$ and enthalpy data for the synthesized phases.

No actinide–borate minerals are known to naturally occur in the environment. One of the first reported synthetic crystalline actinide borate compound $\text{K}_6[\text{UO}_2(\text{B}_{16}\text{O}_{24}(\text{OH})_8)]\cdot 12\text{H}_2\text{O}$ was obtained by evaporation of water at room temperature²⁰. Gasperin and co-workers synthesized U(VI) and Th(IV) borate compounds such as ThB_2O_5 , MgB_2UO_7 and NaBUO_5 using molten B_2O_3 at temperatures above 1000°C ²¹⁻²³. A variety of borate compounds with lanthanides^{24, 25} and, recently, Am(III) and Pu(IV) were prepared by using boric acid flux at moderate temperatures ($\sim 200^\circ\text{C}$)²⁶⁻²⁸. In spite of the increasing number of studies reporting the formation of An– and Ln–borate crystalline compounds, only a very few experimental studies are available so far assessing the formation, potential stability and relevance of these compounds in aqueous systems at lower temperatures (e.g. 25°C).

Note also that so far no systematic study on An(III)-borate interactions affecting solubility and speciation under a large variation of geochemical boundary conditions (pH, [B], [NaCl], [MgCl₂], [CaCl₂]) has been performed.

One of the challenges encountered when quantitatively assessing An–borate interaction is the complex and yet largely unknown aqueous speciation of boron. A number of experimental approaches including potentiometric titrations^{29, 30}, Raman spectroscopy³¹, ¹¹B–NMR³²⁻³⁵, isopiestic measurements^{36, 37} and solubility studies³⁸⁻⁴⁰ have been considered in the literature

to assess the speciation of boron in solution. The available thermodynamic data^{29, 30, 41} allow the calculation of species distribution for some cases, although the accuracy of these calculations at elevated boron and salt concentration (especially in the case of MgCl_2) is importantly hindered. Monomeric species $\text{B(OH)}_3(\text{aq})$ and B(OH)_4^- prevail at low boron concentration under acidic and alkaline pH conditions, respectively (Figure 1a). Due to the neutral character of $\text{B(OH)}_3(\text{aq})$ and the highly delocalized charge in B(OH)_4^- , these monomeric species are expected to have a low tendency to complex hard Lewis acids such as actinide cations⁴². Polyborate species (e.g. $\text{B}_3\text{O}_3(\text{OH})_4^-$, $\text{B}_4\text{O}_5(\text{OH})_4^{2-}$ and $\text{B}_5\text{O}_6(\text{OH})_4^-$, among others) are known to form with increasing boron concentrations (Figure 1b)^{29, 30}. These species have been reported to form stronger complexes with actinides than the corresponding monomeric species^{3, 7}. Note that analogous oligomeric species have been reported for silicium ($\text{Si}_2\text{O}_2(\text{OH})_5^-$, $\text{Si}_3\text{O}_5(\text{OH})_5^{3-}$, $\text{Si}_4\text{O}_7(\text{OH})_5^{3-}$, among others⁵), hence highlighting the similarities existing between B and Si.



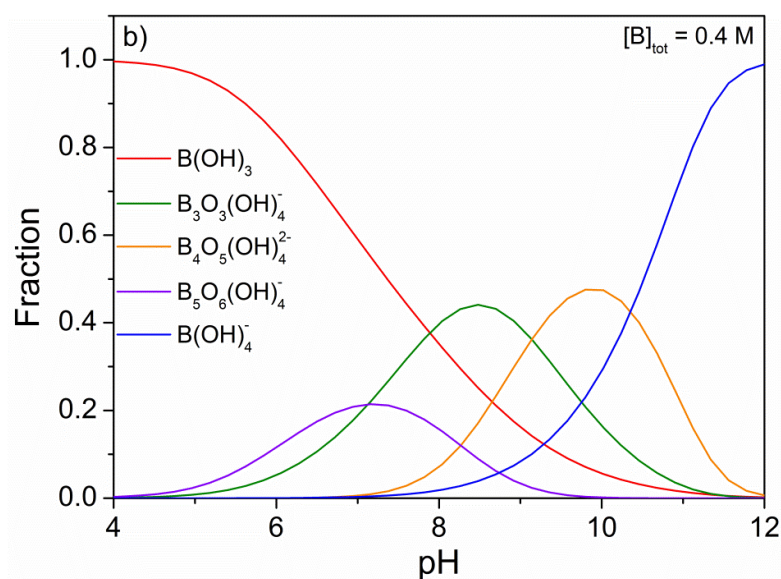


Figure 1. Fraction diagram of aqueous boron species calculated for $4 \leq \text{pH} \leq 12$ at $I = 0$ for a) $[\text{B}]_{\text{tot}} = 0.04 \text{ M}$, and b) $[\text{B}]_{\text{tot}} = 0.4 \text{ M}$. Thermodynamic data used in the calculations as reported in Ingri et al. (1957) and Ingri (1962)^{29, 30}.

The limited experimental data available to assess aqueous boron speciation is especially manifest for elevated ionic strength conditions and MgCl_2 and CaCl_2 brines. Raman studies conducted by Zhihong and co-workers showed a favored formation of polyborates in the presence of high Mg^{2+} concentrations, although no quantitative thermodynamic description was provided by the authors⁴³. The solubility (as equilibrium concentration in saturated solutions) of the systems $\text{CaO-B}_2\text{O}_3\text{-H}_2\text{O}$ and $\text{MgO-B}_2\text{O}_3\text{-H}_2\text{O}$ was intensively investigated in the 40's to 70's by Russian scientists, who reported the formation of several mixed solid phases between these alkaline-earth elements and boron (i.e. $2\text{MgO}\cdot 3\text{B}_2\text{O}_3\cdot 15\text{H}_2\text{O}$, $2\text{CaO}\cdot 3\text{B}_2\text{O}_3\cdot 13\text{H}_2\text{O}$, among others)^{39, 40}. Very recently, Wang and co-workers conducted a very comprehensive literature review with the aim of developing a mixed-solvent electrolyte (MSE) thermodynamic model covering the systems $\text{M}_n\text{O} + \text{B}_2\text{O}_3 + \text{H}_2\text{O}$ (with $\text{M} = \text{Li}, \text{Na}, \text{Ca}, \text{Mg}$ and $n = 1, 2$). In addition to $\text{B(OH)}_3(\text{aq})$, B(OH)_4^- , $\text{NaB(OH)}_4(\text{aq})$ and $\text{LiB(OH)}_4(\text{aq})$ monomeric species, the authors included in their model the polyborate species $\text{B}_2\text{O(OH)}_5^-$, $\text{B}_3\text{O}_3(\text{OH)}_4^-$, $\text{B}_4\text{O}_5(\text{OH)}_4^{2-}$ and $\text{B}_5\text{O}_6(\text{OH)}_6^{3-}$. No Ca-borate or Mg-borate binary aqueous species were considered by the authors in their thermodynamic model⁴⁴. It should be noted that due to the fact that Wang and co-authors use the thermodynamic MSE approach, the results and data selections cannot be transferred to either the SIT⁴⁵ or Pitzer⁴⁶ approaches.

In order to improve the lack of understanding and limited thermodynamic description of the $\text{Ln}^{\text{III}}/\text{An}^{\text{III}}$ -borate system, solubility experiments in combination with spectroscopy and a detailed solid phase characterization (XRD, XPS) were performed in the present study. The work focusses at near-neutral to hyperalkaline NaCl, MgCl_2 and CaCl_2 solutions in the presence of potentially repository-relevant boron concentrations ($4 \times 10^{-3} \text{ M} \leq [\text{B}]_{\text{tot}} \leq 0.4 \text{ M}$). The work especially aims at providing robust upper limits for An(III) concentrations in the presence of borate, valid for source term estimations in performance assessment (PA) exercises for a large variety of geochemical boundary conditions.

2. Experimental

2.1. Chemicals

Crystalline sodium tetraborate $\text{Na}_2\text{B}_4\text{O}_7 \cdot 10\text{H}_2\text{O}(\text{s})$, $\text{MgCl}_2 \cdot 6\text{H}_2\text{O}(\text{s})$, $\text{CaCl}_2 \cdot 2\text{H}_2\text{O}(\text{s})$, $\text{Mg}(\text{OH})_2(\text{s})$ and $\text{Ca}(\text{OH})_2(\text{s})$ were obtained from Merck (p.a.). Aqueous solutions were prepared with purified water obtained from a Milli-Q academic apparatus (Millipore) and purged with argon before use. The pH_c of the different solutions was adjusted with HCl (Titrisol®, Merck), NaOH (Titrisol, Merck), $\text{Ca}(\text{OH})_2$ and $\text{Mg}(\text{OH})_2$ of appropriate ionic strength. In MgCl_2 and CaCl_2 solutions, the maximum pH_c is limited to $\text{pH}_{\text{max}} = 9$ and 12 due to the precipitation and consequent pH-buffering of magnesium and calcium hydroxides or hydroxochlorides, respectively⁴⁷. Sufficiently long equilibration time (~1 month) was allowed for all borate systems in dilute to concentrated saline solutions before the addition of $\text{Nd}(\text{OH})_3(\text{am})$ (solubility) and Cm(III) (TRLFS). This was especially important in the case of Cm(III)–TRLFS, where extensive evolution of the Cm(III) species was observed with time. The long-lived curium isotope ^{248}Cm ($t_{1/2} = 3.4 \times 10^5$ years) was used for the TRLFS experiments. The stock solution used in the experiments (2×10^{-5} M Cm(III) in 0.1 M HClO_4) had an isotopic composition of 89.7% ^{248}Cm , 9.4% ^{246}Cm , 0.4% ^{243}Cm , 0.3% ^{244}Cm and 0.1% ^{247}Cm .

2.2. pH measurements

A combination glass pH electrode (type ROSS, Orion), freshly calibrated against dilute standard pH buffers (pH 7–13, Merck), was used to determine the molar H^+ concentration, $[\text{H}^+]$ (with $\text{pH}_c = -\log[\text{H}^+]$). In salt solutions of ionic strength $I \geq 0.1$ M, the measured pH (pH_{exp}) is an operational apparent value related to $[\text{H}^+]$ by $\text{pH}_c = \text{pH}_{\text{exp}} + A_c$, where A_c is given as a function of the NaCl, MgCl_2 and CaCl_2 concentration⁴⁷. This approach is equivalent to calibrating the electrode vs. standard solutions with fixed proton concentrations at constant background electrolyte concentrations, and relates the potential measured in the samples to the proton concentrations on a molar scale. The average deviation between the $-\log[\text{H}^+]$ values determined with ROSS electrodes was 0.01–0.02 depending on the ionic strength of the solution.

2.3. Solid phase preparation and solubility measurements

All solubility experiments were performed in a glovebox under an argon atmosphere at $22 \pm 2^\circ\text{C}$. Solubility samples in NaCl, MgCl₂ and CaCl₂ solutions were prepared from undersaturation in polyethylene vials with 15-20 mL matrix solution and about 10 mg of Nd(OH)₃(am). Amorphous Nd(III) hydroxide used in the solubility experiments was prepared by hydration of crystalline neodymium hydroxide (Nd₂O₃(cr), Merck) in Milli-Q water under an argon atmosphere⁴⁸. The complete transformation of the oxide into the hydroxide phase was confirmed by XRD (JCPDF file No: 70-0215, JCPDS 2001). For the synthesis of crystalline Nd[B₉O₁₃(OH)₄], Nd₂O₃ and H₃BO₃ were taken as starting materials in a molar ratio 1:15. The mixture was placed in a Teflon liner and sealed in a hydrothermal reactor. The reactor was heated to 220°C for 3 days, and let cool down to room temperature in another 2 days. Excess boric acid (H₃BO₃) was washed out with hot water (90°C). The purity of the material obtained was checked with powder X-ray diffraction.

A detailed list of all the solubility experiments prepared is provided in Table 1.

Table 1. Experimental conditions considered in the Nd(III) solubility experiments.

Initial solid phase	Background electrolyte	Salt concentration (M)	[B] _{tot} (M)	pH _c	Equilibration time
Nd(OH) ₃ (am)	NaCl	0.1 M, 1.0 M, 5.0 M	0.004 M, 0.04 M, 0.16 M	7-13	7-142 days
Nd[B ₉ O ₁₃ (OH) ₄]	NaCl	0.1 M, 5.0 M	0.16 M	6-9	7-108 days
Nd(OH) ₃ (am)	MgCl ₂	0.25 M, 1.0 M, 3.5 M	0.004 M, 0.04 M, 0.16 M, 0.4 M	6-9	7-72 days
Nd[B ₉ O ₁₃ (OH) ₄]	MgCl ₂	0.25 M, 3.5 M	0.16 M	6-9	7-108 days
Nd(OH) ₃ (am)	CaCl ₂	0.25 M, 1.0 M, 3.5 M	0.004 M, 0.04 M	8-12	7-142 days

Boron concentrations in MgCl₂, NaCl and CaCl₂ solutions were restricted to 0.4 M, 0.16 M and 0.04 M, respectively. The limitations in solubility observed for these systems are likely

related with the formation of stable Mg-, Na- and Ca-borate solid phases (Wang et al., 2013). Preliminary spectroscopic experiments (Cm(III)-TRLFS) conducted with freshly prepared borate solutions showed Cm(III)-borate complex formation with pronounced kinetic effects, which decreased notably with the pre-equilibration of borate in the corresponding saline solution. Consequently, the boron containing saline solutions were equilibrated for at least 2 weeks before the addition of Nd(OH)₃(am). Nd(III) concentration and pH_c of the solubility samples were monitored at regular time intervals for up to 142 days. The concentration of Nd(III) in the aqueous solution was quantified by ICP-MS (Thermo scientific X-Series II) after phase separation by 10 kD ultrafiltration (~1.5 nm, Pall Life Sciences). The detection limit of the ICP-MS for Nd(III) varied between 10⁻⁹-10⁻¹⁰ mol·L⁻¹, depending upon salt concentration in the original sample and the required dilution steps. The analytical uncertainties of the ICP-MS analyses are 5-10%. The outcome of these solubility studies was compared with previous solubility experiments in borate-free NaCl, MgCl₂ and CaCl₂ solutions, as well as with thermodynamic calculations using thermodynamic and activity models reported by Neck and co-workers⁴⁸.

2.4. Solid phase characterization

The solid phase of selected solubility samples was characterized by X-ray diffraction (XRD) and X-ray photoelectron spectroscopy (XPS). A small amount (~1 mg) of the solid was separated from the solution by centrifugation (4000 g) in the glovebox and washed 3 times with ethanol (2 mL) under an Ar-atmosphere to remove traces of the matrix solution (NaCl, MgCl₂ or CaCl₂) which would interfere with the XRD analysis. The prepared solid was used for XRD analysis with a Bruker D8 Advance diffractometer (Cu K α radiation) equipped with a Sol-X detector. XRD data were collected within $5^\circ \leq 2\Theta \leq 60^\circ$, with a step size of 0.04 $^\circ$ and 6 s accumulation time per step to allow for reliable counting statistics. Solid samples for XPS analysis were prepared using the same approach as described for XRD, although the amount of sample was significantly reduced (10-50 μ g). After drying, the washed solid phase was pressed on an indium foil and analyzed with an XP spectrometer (ULVAC-PHI, Inc., model PHI 5000 VersaProbe II) equipped with a standard dual anode X-ray source (Mg K α (1253.6 eV), Al K α (1486.6 eV)), and with a scanning microprobe X-ray source (monochromatic Al K α). Calibration of the binding energy scale was performed using well-established binding energies of elemental lines of pure metals (monochromatic Al K α : Cu

$2p_{3/2}$ at 932.62 eV, Au $4f_{7/2}$ at 83.96 eV)⁴⁹. Standard deviations of binding energies of isolating samples were within ± 0.2 eV. Survey scans were recorded with a source power of 50 W of the scanning microprobe X-ray source and a pass energy of 187.85 eV of the analyzer, step size 0.8 eV, to identify the elements and to determine their atomic concentrations at the sample surface. Survey scans were recorded to identify the elements and to determine their atomic concentrations. To retrieve information about the chemical state of the elements, narrow scan spectra of elemental lines were recorded at a pass energy of 23.5 eV, step size 0.1 eV. All spectra were charge referenced to the C 1s elemental line of hydrocarbon (C_xH_y) at 284.8 eV.

2.5. Cm(III) TRLFS experiments

Time resolved laser fluorescence spectroscopy (TRLFS) experiments were performed with 1×10^{-7} M Cm(III) per sample and well-defined concentration of NaCl, $CaCl_2$ and $MgCl_2$ background electrolytes. Total boron concentrations $[B]_{tot}$ ranged from 0.004 M to 0.4 M. Spectra in NaCl and $MgCl_2$ systems were collected at $pH_c = 8.0 \pm 0.1$, whereas spectra in $CaCl_2$ were collected at $pH_c = 8.0 \pm 0.1$ and 12.0 ± 0.1 . After two weeks equilibration time the Cm(III) was spiked to the matrix solutions. The samples were measured within 2 hours after the Cm(III) addition. Measurements with longer equilibration times (up to 2 days) did not show any relevant kinetic effect on the fluorescence spectra. A detailed list of all investigated samples is given in Table 2. Single emission spectra and fluorescence lifetimes were obtained.

Table 2. Experimental conditions in the Cm(III)–TRLFS experiments.

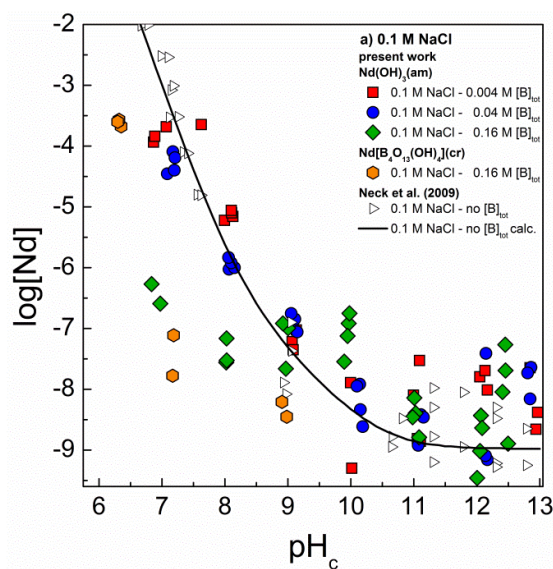
Background electrolyte	Salt concentration (M)	$[B]_{tot}$ (M)	pH_c
NaCl	0.1 M, 5.0 M	0.004 M, 0.04 M, 0.16 M	8.0 ± 0.1
$MgCl_2$	0.25 M, 3.5 M	0.04 M, 0.16 M, 0.4 M	8.0 ± 0.1
$CaCl_2$	0.25 M, 3.5 M	0.004 M, 0.04 M	8.0 ± 0.1 , 12.0 ± 0.1

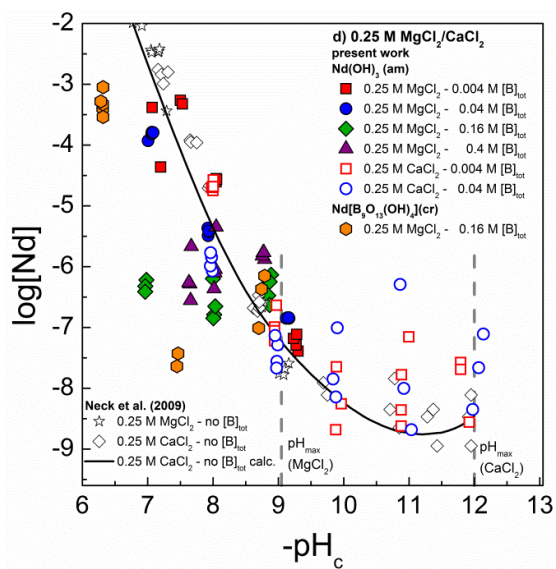
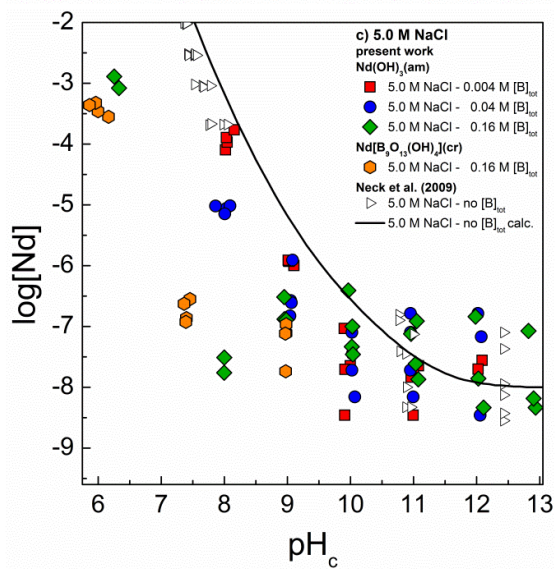
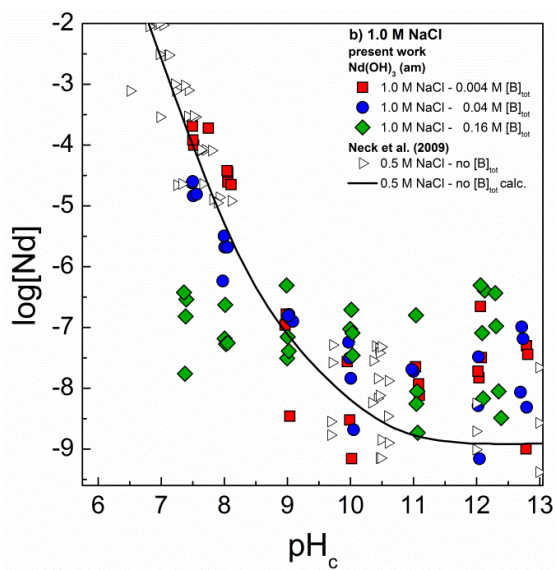
TRLFS spectra were measured with a Nd:YAG pumped dye laser system (Surelite II Laser, Continuum) at a repetition rate of 10 Hz and a maximum laser energy of 3.5 mJ. Spectra were recorded 1 μ s after the exciting laser pulse in a time window of 1 ms at $\lambda_{\text{ex}} = 396.6$ nm (laser dye: Exalite 398). A detection system, consisting of a Shamrock spectrograph (A-SR-303i-B, Andor Technology) and an ICCD camera (iStar ICCD, Andor Technology), was used. Fluorescence lifetime measurements were performed by monitoring the fluorescence emission as a function of the delay time between the laser pulse and the camera gating. Delay times were varied up to 500 μ s with delay steps between 10-15 μ s.

3. Results and discussion

3.1. Solubility of $\text{Nd}(\text{OH})_3(\text{am})$ in the presence of borate

Figure 2 shows the experimental solubility data of Nd(III) determined in 0.1 M, 1.0 M, 5.0 M NaCl and 0.25 M, 1.0 M, 3.5 M MgCl_2 and CaCl_2 solutions in the presence of $0.004 \text{ M} \leq [\text{B}]_{\text{tot}} \leq 0.4 \text{ M}$. Note that only data in equilibrium conditions are plotted in the figure. Figure 2 also shows the solubility data reported by Neck and co-workers in the absence of borate under analogous pH and ionic strength conditions, as well as the solubility curve for $\text{Nd}(\text{OH})_3(\text{am})$ solid phase in systems with absence of complexing ligands, calculated with the thermodynamic and activity models reported by these authors⁴⁸. In the case of 0.1 M, 5.0 M NaCl and 0.25 M, 3.5 M MgCl_2 systems (Figure 2a, 2c, 2d and Figure 2f), undersaturation solubility data obtained with $\text{Nd}[\text{B}_9\text{O}_{13}(\text{OH})_4]$ and $[\text{B}]_{\text{tot}} = 0.16 \text{ M}$ are also provided.





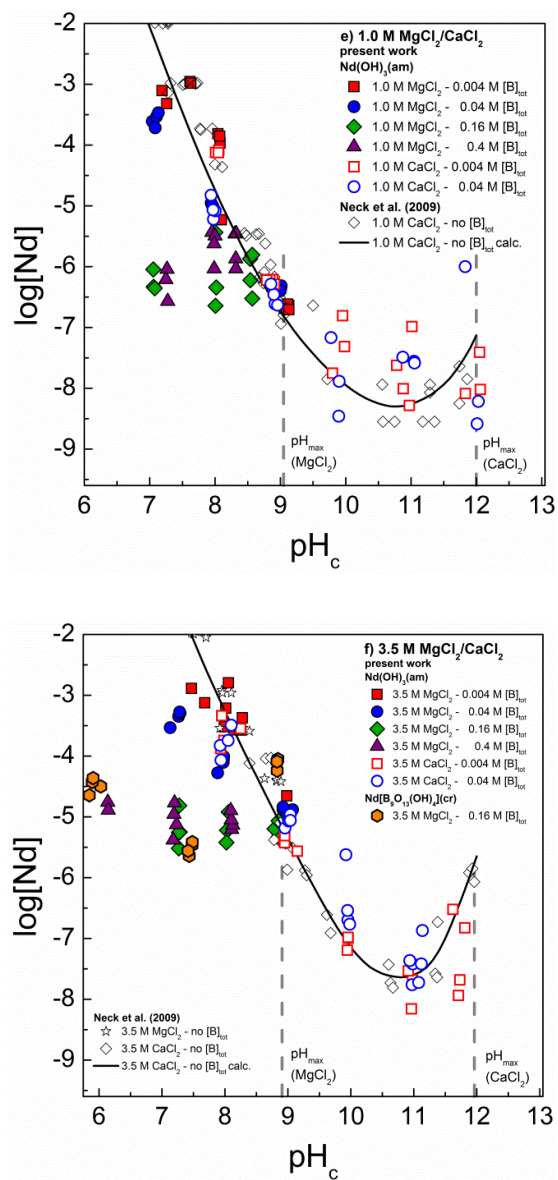


Figure 2. Solubility of $\text{Nd}(\text{OH})_3(\text{am})$ in the presence of $0.004 \text{ M} \leq [\text{B}]_{\text{tot}} \leq 0.4 \text{ M}$ in 0.1 M, 1.0 M and 5.0 M NaCl solutions (a,b,c) and 0.25 M, 1.0 M and 3.5 M MgCl_2 and CaCl_2 solutions (d,e,f). Comparison with experimental (open symbols, black) and calculated (solid line) solubility data in the absence of borate as reported in Neck et al. (2009)⁴⁸.

No significant effect of borate on Nd(III) solubility is observed in near neutral to slightly alkaline pH values ($7 \leq \text{pH}_c \leq 9$) and $[\text{B}]_{\text{tot}} \leq 0.04 \text{ M}$ (dilute salt systems: 0.1 and 1.0 M NaCl; 0.25 M MgCl_2) or $[\text{B}]_{\text{tot}} \leq 0.004 \text{ M}$ (concentrated salt systems: 5.0 M NaCl; 1.0 and 3.5 M MgCl_2). Under these conditions, the concentration of Nd(III) is in good agreement with borate-free solubility data obtained under analogous pH_c and ionic strength⁴⁸. A significant decrease in Nd(III) concentration occurs for all the systems above the indicated $[\text{B}]_{\text{tot}}$. The

drop in solubility is completed at $[B]_{\text{tot}} \sim 0.16\text{--}0.4$ M, where the slope of the solubility curve has changed from -2 to approximately 0 . This observation clearly indicates the transformation of $\text{Nd}(\text{OH})_3(\text{am})$ into a borate-bearing solid phase. After an equilibration time of 72 to 142 days (depending upon salt system), the measured Nd(III) concentrations remain constant at $\sim 10^{-6.5}$ M (in 0.25 M MgCl_2) to 10^{-5} M (in 3.5 M MgCl_2). These solubility limits are more than three orders of magnitude lower than those observed in the absence of borate, as summarized in Table 3. A similar magnitude decrease in Nd(III) solubility is also noted in the NaCl solutions, although the overall solubility is slightly lower. These observations indicate that, as in the case of borate-free systems, increasing MgCl_2 concentrations and resulting high ionic strength enhances significantly the solubility of Nd(III) in the presence of borate. In contrast to NaCl and MgCl_2 systems, no (or very limited) effect of borate on Nd(III) solubility is observed in CaCl_2 solutions, very likely due to the lower boron solubility in this background electrolyte limited to about $[B]_{\text{tot}} \leq 0.04$ M.

Table 3. Comparison of experimental Nd(III) concentrations at $[B]_{\text{tot}} \geq 0.16$ M and calculated Nd(III) concentrations in borate-free NaCl and MgCl_2 solutions.

Matrix	pH_c	$\log [\text{Nd}]$		$\Delta \log\text{-units}$
		borate free ⁴⁸	$[B]_{\text{tot}} \geq 0.16$ M	
0.1 M NaCl	7.1	-3.0	-6.6	3.3
1.0 M NaCl	7.3	-3.4	-7.7	3.3
5.0 M NaCl	8.0	-3.2	-7.8	4.6
0.25 M MgCl_2	7.0	-2.7	-6.4	3.7
1.0 M MgCl_2	7.3	-2.9	-6.6	3.7
3.5 M MgCl_2	7.2	-1.3	-5.5	4.2

The Nd(III) solubility experiments described above were complemented with a series of undersaturation solubility experiments using a well-defined Nd–borate solid phase $\text{Nd}[\text{B}_9\text{O}_{13}(\text{OH})_4](\text{cr})$. The measured Nd(III) solubility of the Nd–borate phases agrees very well with the data measured for $\text{Nd}(\text{OH})_3(\text{am})$ in the presence of $[B]_{\text{tot}} = 0.16$ M, which suggests that similar processes or solid phases are controlling the solubility in both systems.

Very scattered solubility data are obtained under hyperalkaline conditions ($\text{pH}_c \geq 10$). Similar observations have been reported previously for Nd(III) and Th(IV) in the absence of boron^{48, 50}, and likely correspond to a combination of factors such as very low concentrations of Nd and Th in solution (close to the detection limit of ICP–MS), tendency of neutral species to sorb (i.e. $\text{Nd}(\text{OH})_3(\text{aq})$, $\text{Th}(\text{OH})_4(\text{aq})$), and presence of colloidal nanoparticles not retained in the 10 kD filtration step. A slight increase in Nd(III) solubility compared to the borate free data could be claimed for some of the samples with higher $[\text{B}]_{\text{tot}}$ in this pH region, especially in the case of 0.1 M and 1.0 M NaCl systems (Figure 2 a and 2b). Provided the very large scattering in the measured concentration of Nd, the absence of a relevant borate effect on Nd(III) solubility above $\text{pH}_c = 9$ is proposed for both NaCl and CaCl_2 solutions. This observation is interpreted by a decreased interaction between Nd(III) and boron due to the enhanced hydrolysis of Nd(III) with increasing pH.

XRD diffractograms obtained for selected solid phases are shown in Figure 3. In all cases, these patterns agree very well with those reported for $\text{Nd}(\text{OH})_3(\text{am})$ (JCPDF file No: 70-0215, JCPDS 2001), thus providing no indication of a solid phase transformation taking place in the presence of borate by a mechanism leading to bulk crystalline secondary alteration phases. On the other hand, XPS analyses of solubility samples with $[\text{B}]_{\text{tot}} \geq 0.16$ M confirm the presence of a borate-bearing secondary phase on the surface of $\text{Nd}(\text{OH})_3(\text{am})$ (Figure 4). Based on these observations and the solubility data, it can be concluded that a borate-bearing Nd-surface coating is controlling the solubility of Nd(III) under these conditions. Similar XPS spectra were obtained in the case of $\text{Nd}[\text{B}_9\text{O}_{13}(\text{OH})_4](\text{cr})$. These observations can be explained considering either that the solid phase transformation taking place at room temperature leads to a similar Nd–borate structure as $\text{Nd}[\text{B}_9\text{O}_{13}(\text{OH})_4](\text{cr})$, or that a similar coating on both initial Nd solid phases is forming in boron-bearing saline solutions. Note that XRD is a bulk-sensitive technique which cannot account for surface coatings or presence of amorphous phases, whereas XPS provides information from ~ 0.9 to ~ 2.7 nm depth (in the configuration considered in this study, see section 2.3).

Note also that the formation of a Eu(III)–borate solid phase under similar conditions as those investigated in the present study ($\text{pH} = 6$, $[\text{B}]_{\text{tot}} \geq 0.3$ M) was recently reported by Schott et al.⁷. The authors provided evidence (solid-phase TRLFS, IR) of the formation of a distinct Eu(III)–borate solid phase, whose amorphous character was also highlighted by the absence of relevant XRD reflections.

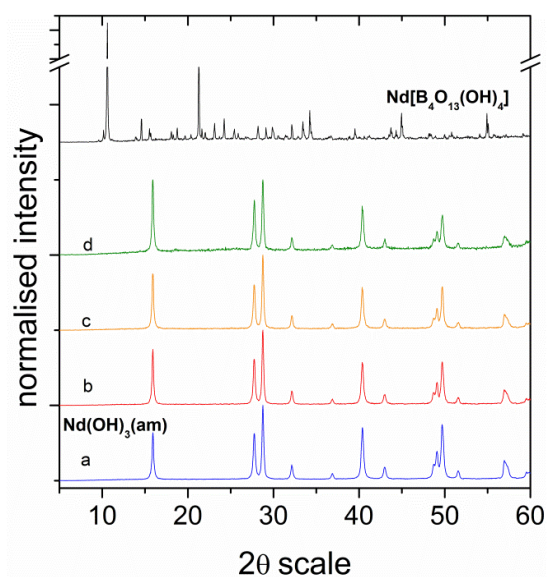


Figure 3. XRD pattern of initial $\text{Nd}(\text{OH})_3$ (am) (a) and $\text{Nd}(\text{OH})_3$ (am) alteration phases from solubility experiments in 0.1 M NaCl (b), 5.0 M NaCl (c) and $[\text{B}]_{\text{tot}} = 0.16$ M and 3.5 M MgCl_2 (d) and $[\text{B}]_{\text{tot}} = 0.4$ M at pH_c 7–8 and crystalline $\text{Nd}[\text{B}_9\text{O}_{13}(\text{OH})_4]$ (cr).

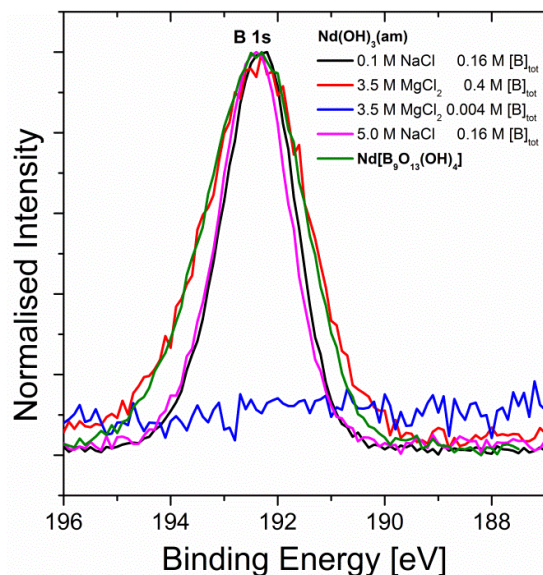


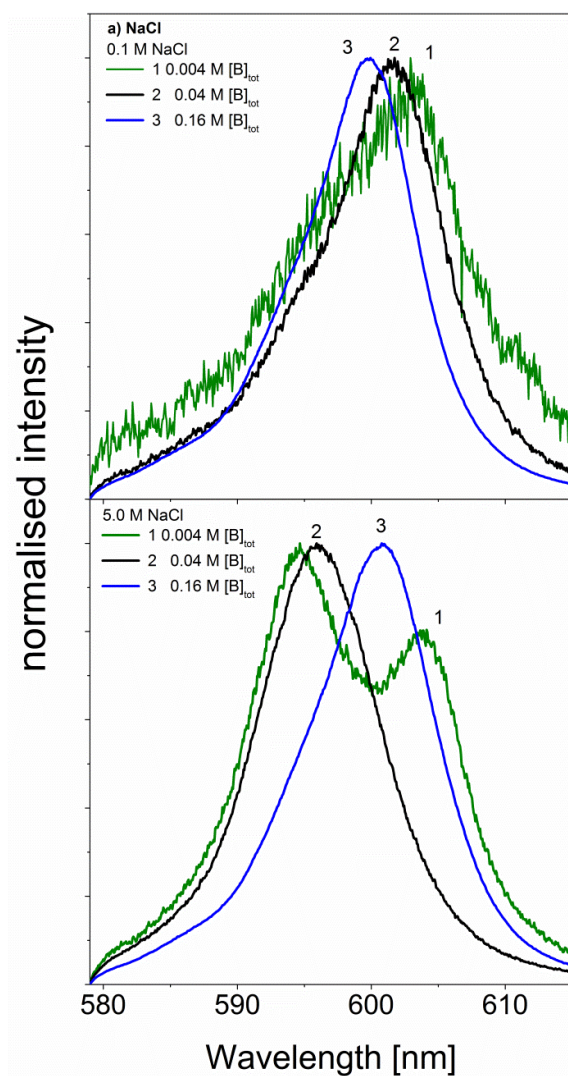
Figure 4. Narrow scan of the Cl 2p and B1s spectra for Nd(III) solid phases in NaCl and MgCl_2 solutions at $\text{pH}_c = 7-8$ with various boron concentrations.

In summary, the experimental data generated in the present work shows that no significant increase in Nd(III) solubility is induced by borate, but instead a very relevant decrease is observed for $[\text{B}]_{\text{tot}} \geq 0.04$ M. According to these results, the thermodynamic model derived by Neck et al.⁴⁸ can be considered to provide reliable upper limit concentrations for trivalent

actinides in performance assessment calculations. The distinct decrease of up to 4.5 orders of magnitude in the Nd(III) concentration at pH_c 7–8 and $[\text{B}]_{\text{tot}} \geq 0.04 \text{ M}$ (for 0.1 M and 1.0 M NaCl $[\text{B}]_{\text{tot}} \geq 0.16 \text{ M}$) together with a clear change of the slope of the solubility curve indicate a transformation of the initial solid phase to a less soluble Nd-borate solid phase. The formation of An(III)–borate solid phases with significantly lower solubility compared to the corresponding hydroxides can be considered as a (so far unknown) An(III) retention mechanism relevant for nuclear waste disposal in borate-rich saline systems.

3.2. Cm(III)–TRLFS in the presence of borate

Fluorescence emission spectra of Cm(III) were measured with varying boron concentrations (see Table 2) in 0.1 M–5.0 M NaCl and 0.25 M–3.5 M CaCl₂ / MgCl₂ solutions at pH_c = 8. The normalised spectra are presented in Figure 5. In CaCl₂ solutions additional spectra with boron concentrations from 0.004 and 0.04 M at pH_{max} ~12 were taken and are shown in Figure 6. Fluorescence decay measurements of spectra in NaCl, CaCl₂ and MgCl₂ solutions with varying boron concentration at pH_c = 8 were performed. The resulting fluorescence lifetimes are presented in Table 4.



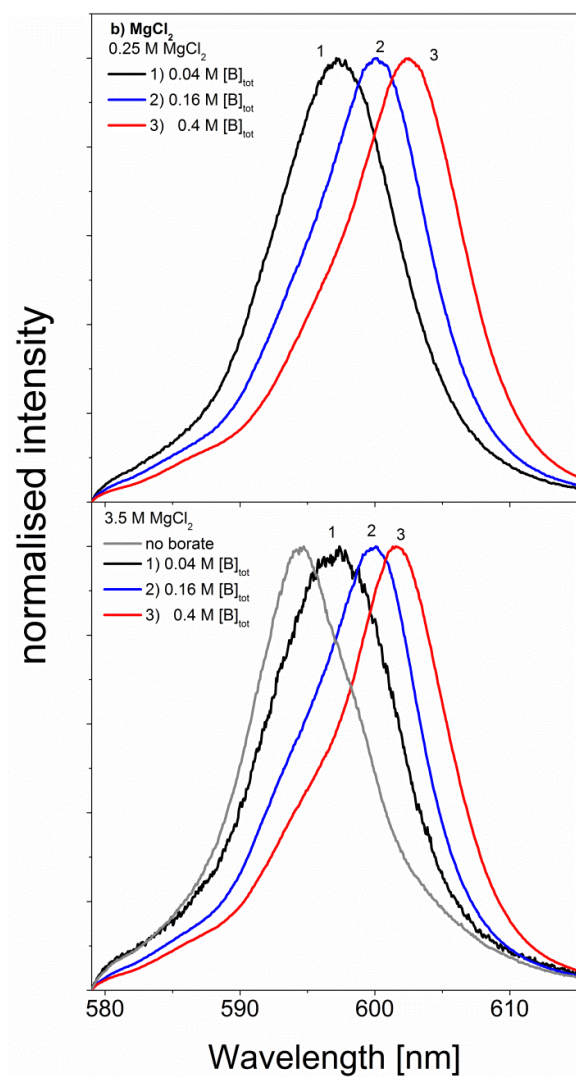


Figure 5. TRLFS emission spectra of Cm(III) in 0.1 M and 5.0 M NaCl solutions (a) and 0.25 M and 3.5 M MgCl₂ solutions (b) at $pH_c = 8$ and various borate concentrations.

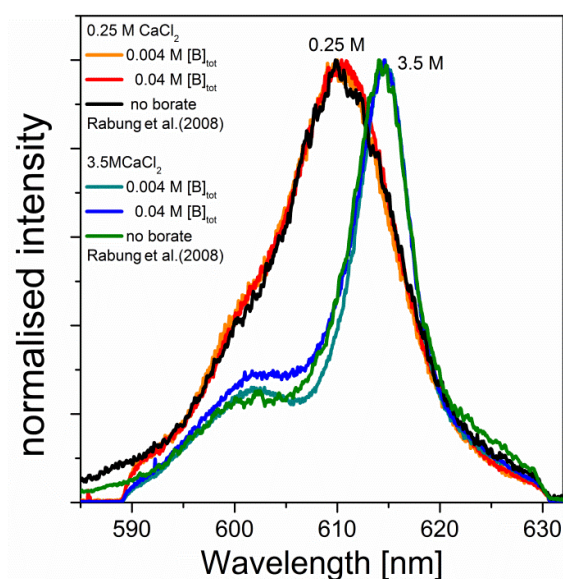


Figure 6. TRLFS emission spectra of Cm(III) in 0.25 M and 3.5 M CaCl₂ at pH_c = 12 and various borate concentrations in comparison with borate-free literature data ⁵¹.

In the near neutral pH region (pH_c = 8) and in the absence of boron, several Cm(III) species are generally expected to be present in solution simultaneously. Their relative contribution depends on the ionic strength and electrolyte composition. Besides the free Cm³⁺ aquo ion, also CmCl²⁺, CmCl₂⁺, Cm(OH)²⁺ and Cm(OH)₂⁺ will contribute in different proportions to the overall Cm(III) species distribution. No significant influence of borates on Cm(III) aqueous speciation can be observed in those samples with low boron concentration ([B]_{tot} = 0.004 M) (Figure 5a). The peak maximum of the scattered spectra in 0.1 M NaCl solution is located at ~603 nm and can be associated mainly with the Cm(OH)₂⁺ complex ⁵². In the absence of complexing ligands other than hydroxyl ions, generally a strong decrease in aqueous Cm concentration is observed due to sorption on surfaces and precipitation as a hydroxide at higher pH. This explains the low intensities and spectral scatter observed for these species. In 5.0 M NaCl two peaks at 594 nm and 604 nm can be found. The first peak can be attributed to the Cm(III) aquo ion (maybe also with small contributions of chloro complexes), the second peak to the second hydrolysis species, as expected at pH_c = 8⁵². These findings in NaCl solutions are in good agreement with the corresponding solubility data (Figure 2) at low borate concentrations.

With increasing boron concentration ([B]_{tot} > 0.004M), the effect of boron on the Cm(III) speciation is obvious in 0.1 M NaCl solutions based on a peak shift to lower wavelengths in

combination with an increased fluorescence intensity of the spectra. A hypsochromic peak shift (shift to shorter wavelengths) appears if complexes with weaker ligands are formed as a consequence of their lower ligand field splitting. In the presence of more than one complexing ligand, weaker complexes will only form if the weak ligand concentration considerably exceeds that of the stronger ligand (i.e. hydroxide anion) which is the case at $\text{pH}_c = 8$ for $[\text{B}]_{\text{tot}} > 0.004 \text{ M}$. At $[\text{B}]_{\text{tot}} = 0.16 \text{ M}$ the competition between borate complexation and hydrolysis leads to a suppression of hydrolysis species and a borate containing Cm(III) complex with a peak maximum at $\sim 600 \text{ nm}$ is formed. A very short fluorescence lifetime ($\tau = 59 \mu\text{s}$) at $[\text{B}]_{\text{tot}} = 0.16 \text{ M}$ is observed. This decrease in the fluorescence lifetime accompanied with a clear shift in the emission spectra in comparison to the Cm(III) aquo ion cannot be explained at the moment. The presence of Cm(III) containing colloids by precipitation of a Cm(III) borate solid, in accordance to the analogue Nd(III)-solubility experiments, could lead to this decrease in the fluorescence lifetime.

In 5.0 M NaCl , the hydrolysis at $\text{pH}_c = 8$ is less pronounced compared to 0.1 M NaCl indicating that considerable amounts of uncomplexed Cm^{3+} are still present. By increasing $[\text{B}]_{\text{tot}}$ to 0.04 M , the hydrolysis peak at $\sim 604 \text{ nm}$ disappears due to competition with borate and a broad peak with a peak maximum at $\sim 596 \text{ nm}$ can be detected consisting of Cm^{3+} emission and a Cm(III) borate component. When further increasing the boron concentration up to 0.16 M , the Cm(III) aquo ion contribution is strongly reduced and the fluorescence peak is shifted to $\sim 601 \text{ nm}$ which can be explained only by the formation of a Cm(III)-borate complex. At the same time the fluorescence lifetime is increased from $77 \mu\text{s}$ at $[\text{B}]_{\text{tot}} = 0.04 \text{ M}$ to $108 \mu\text{s}$ at $[\text{B}]_{\text{tot}} = 0.16 \text{ M}$. Kimura et al. found a linear relation between the number of H_2O entities in the first hydration sphere of the curium ion and the fluorescence decay constant⁵³. According to this relation 4 H_2O molecules are removed from the Cm(III) complex at $[\text{B}]_{\text{tot}} = 0.16 \text{ M}$. One should keep in mind that the influence of high ionic strength on this linear relation is not known at the moment. The peak positions at $[\text{B}]_{\text{tot}} = 0.16 \text{ M}$ for both ionic strengths are rather similar ($\sim 600\text{--}601 \text{ nm}$) which implies that similar Cm-borate species are formed. Note that TRLFS investigations of Cm(III) with inorganic ligands such as Cl^- , CO_3^{2-} and SO_4^{2-} show that peak positions of $\lambda \geq 600 \text{ nm}$ for the most part indicate the coordination of the Cm(III) ion with more than one ligand^{54,55}. Also a mixture of several borate species is possible with a maximum denticity of 1. The fluorescence decay curves show a single averaged exponential decay for all spectra, caused by a faster ligand exchange than the lifetime of the excited state.

Table 4. Fluorescence lifetimes (τ) in NaCl, CaCl₂ and MgCl₂ solutions at pH_c = 8 and various boron concentrations.

Background electrolyte	τ	T	τ	T
	0.004 M [B] _{tot}	0.04 M [B] _{tot}	0.16 M [B] _{tot}	0.4 M [B] _{tot}
0.1 M NaCl	–	77 ± 5	59 ± 5	–
5.0 M NaCl	85 ± 5	77 ± 5	108 ± 5	–
0.25 M CaCl ₂	72 ± 5	78 ± 5	–	–
3.5 M CaCl ₂	73 ± 5	77 ± 5	–	–
0.25 M MgCl ₂	–	85 ± 5	96 ± 5	114 ± 7
3.5 M MgCl ₂	–	87 ± 5	95 ± 5	121 ± 7

In CaCl₂ and MgCl₂ solutions at near neutral pH conditions no hydrolysed Cm(III) species are found in the absence of borate, contrary to the NaCl systems at the same pH⁵⁶. A broad emission peak at ~597 nm at [B]_{tot} = 0.04 M can be observed for both ionic strengths. The peak shift, compared to the borate-free system, indicates the complexation of Cm(III) with borate. At the same time, an increased fluorescence lifetime (77 μ s – 87 μ s, depending on salt system and ionic strength) can be observed compared to the fluorescence lifetime of the Cm(III) Aquoion with 64 ± 3⁵⁷. In contrast to the NaCl system, where Cm(III)-hydrolyses species are present at pH 8, the Cm(III)-borate complexation results in a bathochromic peak shift regarding the Cm(III) aquo ion. With increasing boron concentration the fluorescence emission bands are further shifted to higher wavelengths, which clearly indicates Cm(III) interaction and thus formation of complexes with borate. These pronounced bathochromic peak shifts point to the existence of more than one Cm(III) borate containing complex as it was already concluded for the NaCl system. The bathochromic peak shift of the Cm(III) emission is accompanied with an increase of the fluorescence lifetimes with ascending boron concentrations up to 121 μ s for 3.5 M MgCl₂ and 0.4 M [B]_{tot} (see Table 4). According to the Kimura equation, 3 H₂O molecules are removed in the Cm(III) complexes found in 0.25 M

and 3.5 M MgCl_2 with $[\text{B}]_{\text{tot}} = 0.16$ M, and 4 to 4.5 H_2O molecules for 0.25 M MgCl_2 and 3.5 M MgCl_2 with $[\text{B}]_{\text{tot}} = 0.4$ M, respectively. In MgCl_2 solutions, as already seen in the NaCl system, the formation of Cm -borate species shows no clear dependence on ionic strength within the uncertainty limits of the technique.

Under highly alkaline conditions ($\text{pH}_c = 12$), no influence of borate on the emission spectra can be observed in CaCl_2 solutions and boron concentrations up to 0.04 M (Figure 6). The measured spectra and corresponding fluorescence lifetimes in presence of borate are in good agreement with the borate-free system⁵¹. As previously mentioned borate is a weakly complexing ligand and can only compete with hydrolysis at near-neutral conditions and relatively high borate concentrations, but cannot outcompete hydrolysis under hyperalkaline conditions.

As a consequence of the largely unclear borate speciation at given conditions it is not possible to determine exactly which Cm(III) -borate species are forming and to derive the corresponding pure component spectra required for quantitative spectral deconvolution. However, the present TRIFS study clearly confirms that borate is a weakly complexing ligand and affects Cm(III) and Nd(III) speciation only when present in relatively high concentrations. In all investigated salt systems the peak shifts get more pronounced with increasing boron concentration at similar pH_c , accompanied with increasing fluorescence lifetimes (except for 0.1 M NaCl). Borate interactions with Cm(III) are evident in all studied systems although the exact stoichiometry of the resulting An(III) -borate complexes remains speculative. In our view, in addition to a 1:1 and 1:2 Cm(III) complex with borate, there is also the possible formation of mixed hydroxo-borate or chloro-borate species. According to the fluorescence lifetimes, 4 to 4.5 water molecules are removed from the Cm(III) ion by borate complexation at high boron concentrations (0.4 M). Considering the high complexity of the investigated system a sufficiently justified and convincing quantitative analysis of the spectra is not feasible. The formation of aqueous Cm(III) -borate species provides evidence of a significant tendency towards An(III) -borate interactions that is consistent with the Nd(III) solubility data for NaCl and MgCl_2 solutions at $[\text{B}]_{\text{tot}} \geq 0.04$ M. At this boron concentration the Nd(III) -solubility is controlled by a Nd(III) -borate solid phase and not by Nd(III) hydroxide, which again points at a certain affinity of An(III) towards borates.

4. Conclusions

Ln(III) and An(III) form aqueous complexes with borate in dilute to concentrated NaCl, MgCl₂ and CaCl₂ solutions under near neutral pH conditions and [B]_{tot} ≥ 0.04 M. At [B]_{tot} ≥ 0.16 M and for pH_c = 8, Cm(III)–borate aqueous species outcompete hydrolysis and become predominant. In NaCl and MgCl₂ systems, TRLFS indicates that (at least) two Cm(III)–borate species (maybe 1:1 and 1:2) form, although the exact stoichiometry of the complexation reaction remains unknown. Despite the predominance of Ln^{III}/An^{III}–borate species in solution, no increase in solubility is observed for Nd(OH)₃(am) in the presence of [B]_{tot} ≤ 0.4 M. On the contrary, a clear drop in solubility (2–3 orders of magnitude) occurs at 6 ≤ pH_c ≤ 9, indicating the formation of a new borate-bearing solid phase. This mechanism is confirmed by XPS analysis, which suggests that the newly formed phase occurs as a coating of an unreacted Nd(OH)₃(am) core. The observed significant decrease in solubility related to the formation of secondary An(III)–borate alteration phases represents a hitherto unknown actinide retention mechanism in repository systems at pH_c < 9. No comprehensive thermodynamic evaluation of the chemistry controlling Ln(III)/An(III) interactions in these systems is available so far. This is mostly due to the uncertainties affecting aqueous borate speciation, Ln^{III}/An^{III}–borate aqueous species and solid compounds prevailing in the system. The present study is part of a comprehensive assessment of actinide(III, IV, V, VI) interactions with borate in aqueous systems currently on-going at KIT–INE.

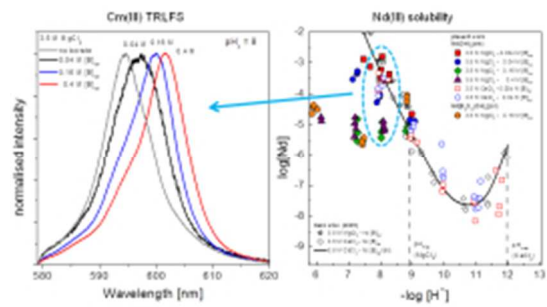
Acknowledgements

The contribution of F. Geyer (KIT–INE), M. Böttle (KIT–INE), N. Fink (KIT–INE) and B. Xiao (FZJ) to analytical methods and preparation of experiments are highly appreciated and gratefully acknowledged. We thank M. Borkowski (LANL–CO) for fruitful discussions on the borate chemistry. This research has received partial funding from the German Federal Ministry of Economics and Technology (BMWi) under the project number: 02E11021. Support for the Los Alamos contributions are provided through the WIPP project (DOE–CBFO). E. Alekseev (FZJ) is supported by the Helmholtz Association within the VH-NG-815 project.

References

1. M. Borkowski, J. Garner, J.-F. Lucchini, D. T. Reed and M. K. Richmann, *Appendix SOTERM-2009 Actinide Chemistry Source Term* LA-UR-13-24559 United States 10.2172/1084512 Tue Oct 01 11:10:19 EDT 2013 LANL English, 2013.
2. C. Bube, V. Metz, E. Bohnert, K. Garbev, D. Schild and B. Kienzler, *Physics and Chemistry of the Earth, Parts A/B/C*, 2013, **64**, 87-94.
3. M. Borkowski, M. Richmann, D. T. Reed and Y. Xiong, *Radiochimica Acta*, 2010, **98**, 577-582.
4. M. Altmaier, X. Gaona and T. Fanghänel, *Chemical reviews*, 2013, **113**, 901-943.
5. R. Guillaumont, F. J. Mompean, T. Fanghänel, J. Fuger, I. Grenthe, V. Neck, D. A. Palmer, M. Illemassène, C. Domenech-Orti, K. Ben Said and M. H. Rand, *Update on the chemical thermodynamics of uranium, neptunium, plutonium, americium and technetium*, Elsevier, Amsterdam, 2003.
6. M. H. Rand, F. J. Mompean, J. Perrone and M. Illemassène, *Chemical thermodynamics of thorium*, Organization for Economic, 2008.
7. J. Schott, J. Kretzschmar, M. Acker, S. Eidner, M. U. Kumke, B. Drobot, A. Barkleit, S. Taut, V. Brendler and T. Stumpf, *Dalton Transactions*, 2014.
8. B. Kienzler, B. Luckscheiter and S. Wilhelm, *Waste Management*, 2001, **21**, 741-752.
9. N. G. Chernorukov, A. V. Knyazev, V. O. Khomyakova and O. V. Nipruk, *Radiochemistry*, 2006, **48**, 18-23.
10. N. G. Chernorukov, A. V. Knyazev and O. V. Kortikova, *Radiochemistry*, 2003, **45**, 475-479.
11. N. G. Chernorukov, A. V. Knyazev, O. V. Kortikova and I. V. Sergacheva, *Russian Journal of General Chemistry*, 2003, **73**, 1167-1173.
12. N. G. Chernorukov, A. V. Knyazev, I. V. Sergacheva and A. V. Ershova, *Radiochemistry*, 2004, **46**, 218-223.
13. N. G. Chernorukov, O. V. Nipruk, A. V. Knyazev and V. O. Khomyakova, *Radiochemistry*, 2003, **45**, 273-275.
14. N. G. Chernorukov, N. N. Smirnova, A. V. Knyazev, M. N. Marochkina, T. A. Bykova and A. V. Ershova, *Russian Journal of Physical Chemistry*, 2006, **80**, 37-41.
15. N. G. Chernorukov, N. N. Smirnova, A. V. Knyazev, M. N. Marochkina and A. V. Ershova, *Russian Journal of Physical Chemistry*, 2006, **80**, 1205-1209.
16. N. G. Chernorukov, N. N. Smirnova, A. V. Knyazev, M. N. Marochkina and A. V. Ershova, *Russian Journal of Physical Chemistry*, 2006, **80**, 1915-1919.
17. N. G. Chernorukov, N. N. Smirnova, A. V. Knyazev, M. N. Marochkina and A. V. Ershova, *Russian Journal of Physical Chemistry A*, 2007, **81**, 683-687.
18. N. V. Karyakin, N. G. Chernorukov, A. V. Knyazev, V. O. Khomyakova and N. N. Smirnova, *Radiochemistry*, 2005, **47**, 136-149.
19. N. Karyakin, N. Chernorukov, A. Knyazev and O. Kortikova, *Russian Journal of Physical Chemistry*, 2003, **77**, 1925-1928.

20. H. Behm, *Acta Crystallographica Section C-Crystal Structure Communications*, 1985, **41**, 642-645.
21. A. Cousson and M. Gasperin, *Acta Crystallographica Section C*, 1991, **47**, 10-12.
22. M. Gasperin, *Acta Crystallographica Section C*, 1987, **43**, 2264-2266.
23. M. Gasperin, *Acta Crystallographica Section C-Crystal Structure Communications*, 1988, **44**, 415-416.
24. L. Y. Li, X. L. Jin, G. B. Li, Y. X. Wang, F. H. Liao, G. Q. Yao and J. H. Lin, *Chem Mater*, 2003, **15**, 2253-2260.
25. P. C. Lu, Y. X. Wang, J. H. Lin and L. P. You, *Chem. Commun.*, 2001, 1178-1179.
26. S. A. Wang, E. V. Alekseev, W. Depmeier and T. E. Albrecht-Schmitt, *Chemical Communications*, 2011, **47**, 10874-10885.
27. M. J. Polinski, S. A. Wang, E. V. Alekseev, W. Depmeier and T. E. Albrecht-Schmitt, *Angewandte Chemie-International Edition*, 2011, **50**, 8891-8894.
28. S. Wang, E. V. Alekseev, W. Depmeier and T. E. Albrecht-Schmitt, *Inorganic Chemistry*, 2011, **50**, 2079-2081.
29. N. Ingri, G. Lagerstrom, M. Frydman and L. G. Sillen, *Acta Chemica Scandinavica*, 1957, **11**, 1034-1058.
30. N. Ingri, *Acta Chem. Scand.*, 1962, **16**, 439-448.
31. T. Hirao, M. Kotaka and H. Kakihana, *Journal of Inorganic & Nuclear Chemistry*, 1979, **41**, 1217-1220.
32. C. G. Salentine, *Inorganic Chemistry*, 1983, **22**, 3920-3924.
33. G. Heller, R. Janda and J. Mathieu, *Inorganica Chimica Acta-Articles*, 1980, **40**, X107-X108.
34. R. K. Momii and Nachtrie.Nh, *Inorganic Chemistry*, 1967, **6**, 1189-&.
35. K. Ishihara, A. Nagasawa, K. Umemoto, H. Ito and K. Saito, *Inorganic Chemistry*, 1994, **33**, 3811-3816.
36. N. P. Nies and R. W. Hulbert, *Journal of Chemical and Engineering Data*, 1967, **12**, 303-313.
37. B. B. Owen, *Journal of the American Chemical Society*, 1934, **56**, 1695-1697.
38. A. Apelblat and E. Manzurola, *Journal of Chemical Thermodynamics*, 2003, **35**, 221-238.
39. A. Nikolaev and A. Chelischeva, *Comp. Rend. Acad. Sci USSR*, 1940, **28**, 127-130.
40. A. G. Kurnakova, *Izvest. Sektora Fiz. Khim. Anal., Inst. Obshchei i Neorg., Akad. Nauk SSSR*, 1947, **15**, 125.
41. A. R. Felmy and J. H. Weare, *Geochimica et Cosmochimica Acta*, 1986, **50**, 2771-2783.
42. R. G. Pearson, *Inorg. Chim. Acta*, 1995, **240**, 93-98.
43. L. Zhihong, G. Bo, L. Shuni, H. Mancheng and X. Shuping, *Spectrochimica acta. Part A, Molecular and biomolecular spectroscopy*, 2004, **60**, 3125-3128.
44. P. Wang, J. J. Kosinski, M. M. Lencka, A. Anderko and R. D. Springer, *Pure and Applied Chemistry*, 2013, None-None.
45. L. Ciavatta, *Ann. Chim.(Rome)*, 1980, **70**, 551-567.
46. K. S. Pitzer, *Activity coefficients in electrolyte solutions*, CRC press, 1991.
47. M. Altmaier, V. Metz, V. Neck, R. Muller and T. Fanghänel, *Geochimica Et Cosmochimica Acta*, 2003, **67**, 3595-3601.
48. V. Neck, M. Altmaier, T. Rabung, J. Lutzenkirchen and T. Fanghanel, *Pure Appl. Chem.*, 2009, **81**, 1555-1568.
49. M. Seah, I. Gilmore and G. Beamson, *Surf Interface Anal*, 1998, **26**, 642-649.
50. M. Altmaier, V. Neck and T. Fanghanel, *Radiochimica Acta*, 2004, **92**, 537-543.
51. T. Rabung, M. Altmaier, V. Neck and T. Fanghänel, *Radiochimica Acta*, 2008, **96**, 551-559.
52. T. Fanghänel, J. I. Kim, P. Paviet, R. Klenze and W. Hauser, *Radiochimica Acta*, 1994, **66-7**, 81-87.
53. T. Kimura, G. R. Choppin, Y. Kato and Z. Yoshida, *Radiochim Acta*, 1996, **72**, 61-64.
54. J. I. Kim, R. Klenze, H. Wimmer, W. Runde and W. Hauser, *Journal of Alloys and Compounds*, 1994, **213-214**, 333-340.
55. T. Fanghänel and J. I. Kim, *Journal of Alloys and Compounds*, 1998, **271-273**, 728-737.
56. M. Herm, Diploma Thesis, Karlsruhe Institute of Technology, 2012.
57. H. Wimmer, R. Klenze and J. I. Kim, *Radiochim. Acta*, 1992, **56**, 79-83.



70x39mm (96 x 96 DPI)